 doi:10.20944/preprints202103.0359.v1

Mechanics Modeling of Residual Stress Considering Effect of Preheating in Laser Powder Bed Fusion

Elham Mirkoohi[1*], Hong-Chuong Tran[2], Yu-Lung Lo[3], You-Cheng Chang[3], Hung-Yu Lin[3], and Steven Y. Liang[1]

[1]Woodruff School of Mechanical Engineering, Georgia Institute of Technology, Atlanta, GA 30332, USA;
[2]Department of Mechanical Engineering, Southern Taiwan University of Science and Technology, Tainan 71005, Taiwan
[3]Department of Mechanical Engineering, National Cheng Kung University, Tainan City, Taiwan 701

*Corresponding Author: Elham Mirkoohi, Elham.mirkoohi@gatech.edu

Abstract
This study aimed at the investigation of the effect of substrate preheating on residual stress in laser powder bed fusion using a physics-based analytical model. In this study, an analytical model is proposed to predict the residual stress through the calculation of preheating affected temperature profile and thermal stress. The effect of preheating is super-positioned with initial temperature in the modeling of temperature profile using a moving heat source approach; the resultant temperature gradient is then employed to predict the thermal stress from a point body load approach. If the thermal stress exceeds the yield strength of the material, then the residual stress under cyclic heating and cooling will be calculated based on the incremental plasticity and kinematic hardening behavior of metal. IN718 is used as a material example to pursue this investigation. To validate the predicted residual stress, experimental measurements are conducted using X-ray diffraction on IN718 samples manufactured via laser powder bed fusion under different process conditions. Results showed that preheating of the substrate could reduce the residual stress in an additively manufactured part due to the reduction in temperature gradient and resultant shrinkage stresses. However, the excessive preheating could have an opposite impact on residual stress accumulation. Moreover, the results confirm that the proposed model is a valuable tool for the prediction of residual stress- eliminating the costly experiments and time-consuming finite element simulations.

Keywords: Preheating; L-PBF; Residual stress; IN718; Analytical modeling; Experimentation

1. Introduction

Metal additive manufacturing (AM) in which the near net shape components are built up from a high precision laser, has become an important technology in the past few years to manufacture 3D components [1]. The metal additive manufacturing can be divided into two main categories of powder feed (PF) system in which the powders are carried out via nozzles; and powder bed fusion (L-PBF) in which the powders are sat on a bed to be melted selectively [2]. The advantages of AM compared to traditional manufacturing are that the components are built directly without the requirement for specific tooling that enhances the geometric freedom of the process, enabling the manufacture of complex geometries, which then can reduce the lead time and cost per part. Moreover, compared to conventional manufacturing methods, L-PBF offers higher energy

Preprints (www.preprints.org) | NOT PEER-REVIEWED | Posted: 15 March 2021 doi:10.20944/preprints202103.0359.v1

efficiency, faster build rates, and larger parts. As a result, L-PBF gaining attention as an assuring technology for the fabrication of large and intricate components for aerospace, marine, and medical companies [3].

The residual stress resulting from rapid heating and cooling cycles in L-PBF is not well understood yet. Each process parameters can considerably change the residual stress distribution. This is a very important issue in additive manufacturing of metallic components since it not only degrades the dimensional accuracy and mechanical performance of the component, but also increases the manufacturing cost due to necessity for post-processing treatments [4]. It is therefore important to understand and control the residual stress by the optimization of process parameters.

Residual stress induced by laser powder bed fusion (L-PBF) can surpass the yield strength of the metal [5]. Such high residual stress buildup could affect the microstructure and mechanical properties of the fabricated part [6]. Various thermal and mechanical treatments are often performed to reduce residual stress. They include in-situ preheating of the substrate in which the part is built on top of it, post-processing heat treatment, peening, and pre-setting [7]. Preheating involves raising the temperature of the base metal in which the part is built on top of it (substrate) above the ambient temperature. Preheating could improve the additive-manufacturability of the parts since it retards the temperature gradient and cooling rates in the metal and heat-affected base metal and reduces the magnitude of shrinkage stresses. Thus, it is an effective mean to reduce residual stress, distortion, metal cracking, and prohibit the failure of the part in service. On the other hand, an excessive amount of preheating could have an opposite impact on final performance of the manufactured part. The excessive amount of preheating could result in segregation of embrittling impurity elements to the grain boundaries. It also causes significant grain coarsening in the melt pool area and heat-affected zone (HAZ) and result in creation of a wider zone of grain boundary liquidation. These partly melted zones have very poor ductility and are quite sensitive to cracking [8]. Therefore, magnitude of the preheating temperature plays an important role on the final performance of the additively manufactured part.

Analytical models play a significant role in the study of thermo-mechanical behavior in metal AM. The rationale for performing analytical modeling of additive manufacturing processes is to reduce the experimentation needed to optimize the process parameters [9]. In addition, it offers high-performance computing. For instance, the simulation of residual stress considering multi-layer and multi-scan aspects of AM process using the proposed model takes less than two and half minutes to be completed using a 2.3 GHz core i5 laptop compared to hours of calculations using finite element modeling since it involves no iteration, nor meshing. Moreover, such models can then be extended to model the microstructure of the additively manufactured part. For example, Tabei *et al.* [10] used the thermo-mechanical analytical model to predict the microstructure of an additively manufactured part, and Ji *et al.* [11] used a similar model to predict the grain size of an additively manufactured part.

Finite element analysis (FEA) has been an active area of research for modeling of AM process. Nick *et al*. [12] used FEA to model the effect of deposition pattern on residual stress on laser deposited 1117 steel. In this modeling, they did not consider the effect of latent heat, the entire layer is heated up and then cooled down after deposition instead of using moving heat source, the effect of layer addition and multi-scan aspect of AM is also not considered. Alimardani *et al.* [13] proposed a numerical model to investigate the effect of pre-heating on residual stress in additive manufacturing of 304 L stainless-steel. They concluded that the pre-heating could reduce the thermal stress and subsequent residual stress. In this modeling, the results are not validated. Chew *et al.* [14] developed a FE model to predict the residual stress in a single and multiple bead laser

Preprints (www.preprints.org) | NOT PEER-REVIEWED | Posted: 15 March 2021 doi:10.20944/preprints202103.0359.v1

deposition. They have validated their results by conducting experimental residual stress using X-ray diffraction. The results showed quantitative agreement with experimental measurements, however, the measurement results are obtained only at the center of clad. Ding *et al.* [15] verified the bulk residual stress distribution simulated by a finite element model using neutron diffraction for samples up to 3 layers. While the predicted and measured residual stresses are in good agreement for the second and third layers, the simulation dramatically underestimated the residual stress for the first layer. Ali *et al.* experimentally investigated the effect of preheating on yield strength and ductility of the Ti6Al4V. They found that increasing the temperature of the bed to 570℃ could improve the yield strength and elongation of the component by 3.2% and 66.6%, respectively [16]. Buchbinder *et al.* investigated the effect of preheating on distortion of the additively manufactured components. They concluded that the preheating of substrate to 250℃ resulted in elimination of distortion from 10.6 mm (without preheating)[17]. Sames *et al.* indicated that the highest stress concentration is located near the interface between substrate and SLM-processed part. These results indicate that the interface between substrate and part is the locations where the part has more possibility to delaminate during SLM process [18].

To the best of authors knowledge there is no work that specifically model the effect of preheating of substrate on residual stress in metal AM and validate that via experimentation.

In the present work, a physics-based analytical model is proposed to investigate the effect of preheating on residual stress in L-PBF. A fully coupled thermo-mechanical model simulates the residual stress distribution using incremental plasticity and kinematic hardening behavior of the metal through the prediction of temperature field by considering the effect of preheating in the modeling by superposing the preheating temperature with initial temperature, and thermal stress using Green's function of stresses due to the point body load. To validate the proposed model, IN718 samples are built via L-PBF process under different process conditions by varying the preheating temperature to 100℃. The X-ray diffraction is then used to measure residual stress of the samples at five different points along the scan direction and build direction. The results showed that preheating could reduce tensile residual stress in an additively manufactured part by the reduction of shrinkage stress. More investigations are conducted at higher preheating temperature by sensitivity analysis. This analysis showed that excessive preheating could have an opposite impact on residual stress, and it is possible that the residual stress increases due to the excessive preheating. A comparison of the predicted and measured residual stress also showed good quantitative and qualitative agreement, which demonstrates that the proposed model can be used to optimize the preheating temperature to reduce the residual stress formation.

2. Methodology

The first step in mechanics modeling of AM process is to predict the temperature field induced by a laser as shown in Figure 1. In this modeling approach, a transient moving point heat source approach [19] is used to predict the temperature field considering part's boundary conditions. To consider the effect of preheating, the constant preheating temperature is added to the moving profile as the following;

$$T_{final} = T - T_{loss} = \frac{P\eta}{4\pi KR(T-T_0)} \times \left\{ \exp\left(\frac{-V(R+x)}{2D}\right) - ls[h(T-T_0) + \varepsilon\sigma(T^4 - T_0^4) + \frac{K(T-T_0)}{R}] \right\} + T_{preheating} \quad (1)$$

Preprints (www.preprints.org) | NOT PEER-REVIEWED | Posted: 15 March 2021 doi:10.20944/preprints202103.0359.v1

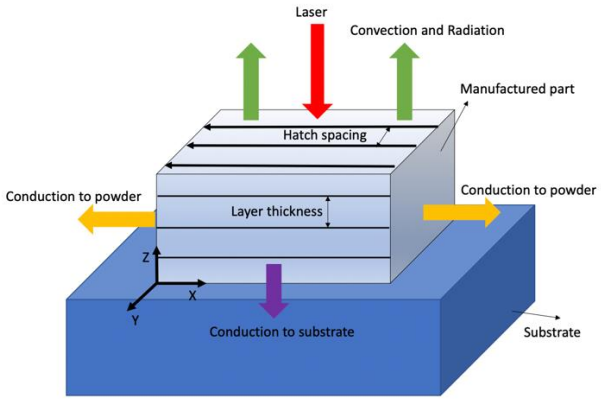

Figure 1. *Heat transfer mechanisms in laser powder bed fusion.*

where P is the laser power, η represents the absorption coefficient, V is scan speed, D is thermal diffusivity, and T_0 is the initial temperature. More explanation and validation of the proposed temperature model can be found in the previous work of these authors in [9, 20].
Calculated temperature gradient from thermal modeling is used as an input to predict the thermal stress in the AM parts as explained in previous work of authors [21] using Green's function of stresses due to the point body load.
In this process high strain, strain rate, and temperature will be generated. The Johnson-Cook materials' consecutive model is used to capture these effects as follows;

$$\sigma = (A + B{\varepsilon_{eff}^{p}}^{n})(1 + Cln\left(\frac{\dot{\varepsilon}_{eff}^{p}}{\dot{\varepsilon}_0}\right))(1 - \left[\frac{T - T_{preheating}}{T_m - T_{preheating}}\right]^{m}) \tag{2}$$

where ε_{eff}^{p} is the effective plastic strain, $\dot{\varepsilon}_{eff}^{p}$ is the effective plastic strain rate, T is the temperature of material, T_m is the melting point of material, and $T_{preheating}$ is the substrate's temperature. The terms A, B, C, n, m and $\dot{\varepsilon}_0$ are the material constant which are listed in Table 1 for IN718 material.

Table 1*. Modified Johnson-Cook parameters for IN718 [22].*

***A*(MPa)**	**B(MPa)**	**C**	**n**	**m**	$\dot{\boldsymbol{\varepsilon}}_{\mathbf{0}}$
980	1370	0.02	0.164	1.03	1

The yielding criterion is obtained for an isotropic material. Kinematic hardening is considered by employing the backstress tensor (α_{ij})

$$F_{yeild} = \frac{3}{2}(S_{ij} - \alpha_{ij})(S_{ij} - \alpha_{ij}) - k^2 = 0 \tag{3}$$

where $S_{ij} = \sigma_{ij} - ({}^{\sigma_{kk}}/_{3})\delta_{ij}$ is the deviatoric stress.
If $F_{yeild} > 0$, incremental plastic strains are calculated and accumulated during the stress history to determine the total plastic strains using modified McDowell algorithm [23].

Preprints (www.preprints.org) | NOT PEER-REVIEWED | Posted: 15 March 2021 doi:10.20944/preprints202103.0359.v1

$$\begin{cases} \frac{1}{E}\left[\dot{\sigma}_{xx} - \upsilon\left(\dot{\sigma}_{yy} - \dot{\sigma}_{zz}\right)\right] + \alpha\Delta T + \frac{1}{h}\left(\dot{\sigma}_{xx}n_{xx} + \dot{\sigma}_{yy}n_{yy} + \dot{\sigma}_{zz}n_{zz} + 2\dot{\sigma}^{*}_{xz}n_{xz}\right)n_{xx} = \\ \psi\left(\frac{1}{E}\left[\dot{\sigma}^{*}_{xx} - \upsilon\left(\dot{\sigma}_{yy} - \dot{\sigma}^{*}_{zz}\right)\right] + \alpha\Delta T + \frac{1}{h}(\dot{\sigma}^{*}_{xx}n_{xx} + \dot{\sigma}_{yy}n_{yy} + \dot{\sigma}^{*}_{zz}n_{zz} + 2\dot{\sigma}^{*}_{xz}n_{xz})n_{xx}\right) \\ \frac{1}{E}\left[\dot{\sigma}_{yy} - \upsilon(\dot{\sigma}_{xx} - \dot{\sigma}_{zz})\right] + \alpha\Delta T + \frac{1}{h}\left(\dot{\sigma}_{xx}n_{xx} + \dot{\sigma}_{yy}n_{yy} + \dot{\sigma}_{zz}n_{zz} + 2\dot{\sigma}^{*}_{xz}n_{xz}\right)n_{yy} = 0 \\ \dot{\sigma}_{yy} = \frac{1}{2}(\dot{\sigma}_{xx} + \dot{\sigma}_{zz}) \end{cases} \quad (4)$$

where, $\dot{\sigma}^{*}_{xx}, \dot{\sigma}^{*}_{zz}, \dot{\sigma}^{*}_{xz}$ are the elastic thermal stresses calculated from [21]. In McDowell model [5], a hybrid function (ψ) is proposed, which depends on the instantaneous value of the modulus ratio h/G as;

$$\psi = 1 - \exp\left(-\xi\frac{3h}{2G}\right) \quad (10)$$

where $\xi = 0.15$ is the algorithm constant, h is the plastic modulus, and $G = E/(2(1+\upsilon))$is the elastic shear modulus. Three systems of equations are solved simultaneously for $\dot{\sigma}_{xx}$, $\dot{\sigma}_{yy}$, and $\dot{\sigma}_{zz}$ for each elastic-plastic increment of strain [5].

3. Experimental Procedure

The Nd: YAG laser with the laser spot size of D4sigma = 54 µm and laser power of 50 W to 400 W is set up on a commercial Tong Tai AM250 SLM machine to manufacture high-density components using variable pre-heating temperatures. The IN718 powders with the powder size distribution of d_{10} = 17.51 µm ; d_{50}= 31.44 µm; d_{90}= 52.21 µm is used. The range of scan speed varies between 100 mm/s to 2000 mm/s. The processing conditions used to fabricate samples are listed in Table 2. To make sure that the selected process parameters would result in a high-density sample, the density of the fabricated samples is measured and listed in Table 3. For measuring the density, each sample was sawed in half. Then, the obtained cross-sections were polished, and their images were taken by a digital camera attached to the microscope. For each sample, the images were captured at five different locations of the cross-section, and the ImageJ software was employed to calculate the relative density by evaluating the ratio between total pore areas and the total cross-sectional area. The calculated relative density from the five images was used to determine the mean value of the relative density of the fabricated samples. Figure 2(a) and 2(b) shows the cross-section images corresponding to the parameters for sample 1 and 2 specified in Table 2, respectively. The statistical results of relative density corresponding to each set of polished samples are shown in Table 3.

In these fabricated samples, the laser power, scan speed, layer thickness, and scan pattern are kept the same, and pre-heating condition is changed to investigate the impact of pre-heating on residual stress. For each set of parameters specified in Table 2, there were three samples fabricated. The as-build samples were then removed from the base plate using the electrical discharge machining (EDM).

Preprints (www.preprints.org) | NOT PEER-REVIEWED | Posted: 15 March 2021 doi:10.20944/preprints202103.0359.v1

Table 2. *Process Parameters Designed for the fabrication of IN718 specimens using L-PBF.*

No.	Laser power (W)	Scanning speed (mm/s)	Powder layer thickness (µm)	Hatch spacing (µm)	Number of scans	Pre-heating (˚C)	Rotation angle of scan vector between layers (˚)
1	150	600	30	100	50	No	67
2	150	600	30	100	50	100	67

Table 3. *Measured density of fabricated samples.*

No.	Average Density	Standard Deviations
1	99.96 %	0.017%
2	99.94%	0.02%

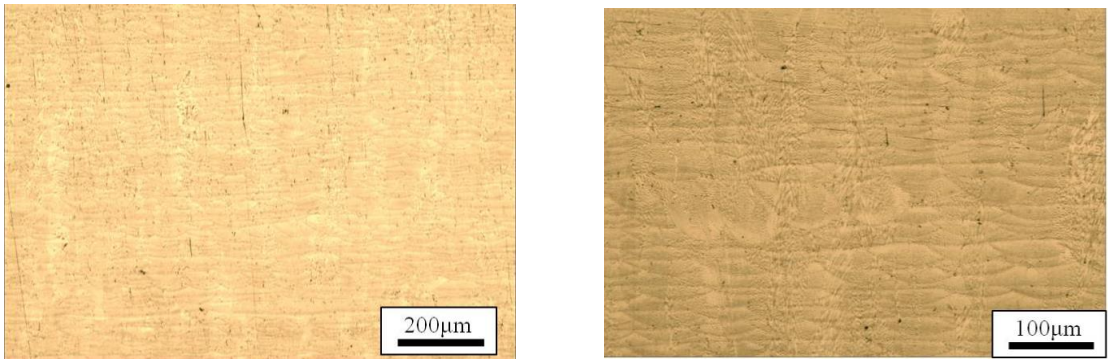

(a) (b)

Figure 2. *Polished cross sections corresponding to two different processing conditions (a) Sample No.1; (b) Sample No.2*

The residual stress on the side walls of the samples, as illustrated in Figure 3, was measured by a commercial X-Ray Diffractions machine (D8 Discover Bruker) using the $sin^2\Psi$ method [24, 25]. The coordinate and location of measured points are shown in Table 4. For each point shown in Figure 3, residual stresses along the build direction (z direction), and along the scan direction (x direction) were measured. The parameters for XRD measurement are specified in Table 5. It is noted that for each set of parameters and each point shown in Figure 3, the XRD measurements were performed on three fabricated samples and the results were averaged.

Preprints (www.preprints.org) | NOT PEER-REVIEWED | Posted: 15 March 2021 doi:10.20944/preprints202103.0359.v1

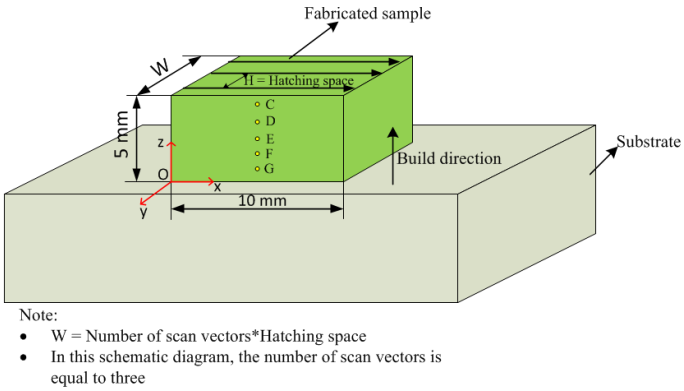

***Figure 3**. Schematic diagram illustrating the definition of processing parameters.*

***Table 4.** Coordinates of the measured points using XRD.*

C	**x = 5 mm; y = 0; z = 4.5 mm**
D	x = 5 mm; y = 0; z = 3.5 mm
E	x = 5 mm; y = 0; z = 2.5 mm
F	x = 5 mm; y = 0; z = 1.5 mm
G	x = 5 mm; y = 0; z = 0.5 mm

***Table 5.** Parameters for XRD measurements*

Focus	**1.0 mm**
Radiation	Cu Kα
Lattice plane (hkl) [25]	{411}
2Θ	145 º
Ψ-tilting	0º to 45º in 6 steps each
Young modulus [26]	199,955 MPa
Poisson ration [26]	0.29

4. Results and Discussion

The proposed thermo-mechanical model calculates the residual stress from incremental plasticity approach in the metal additive manufacturing process through the prediction of temperature profile and thermal stress as explained in the methodology section. A moving point heat source approach is employed to predict the temperature field by considering the effect of temperature dependent material properties of IN718 samples as listed in Table 6. In addition, the effects of multi-layer and multi-scan aspects of L-PBF process, the heat loss due to convection and radiation from boundaries, as well as energy needed for solid state phase change are considered in the modeling of temperature field.

Preprints (www.preprints.org) | NOT PEER-REVIEWED | Posted: 15 March 2021 doi:10.20944/preprints202103.0359.v1

Table 6. *Temperature dependent material properties of IN718 (Temperature is in* ℃.

Density g/cm^3	
$\boldsymbol{\rho = 8.19 - 39.2 \times 10^{-2} T}$	25< T ≤1170
$\boldsymbol{\rho = 7.40 - 88.0 \times 10^{-2} (T - 1200)}$	$\boldsymbol{T > 1170}$
Thermal conductivity W/m℃	
$\boldsymbol{k = 39.73 - 24.0 \times 10^{-3}\ T + 2 \times 10^{-3}\ T^{-2}}$	$\boldsymbol{25 < T < 1170}$
$\boldsymbol{k = 29.6}$	$\boldsymbol{T > 1170}$
Specific heat J/kg℃	
$\boldsymbol{C_p = 420.24 + 0.026T - 4 \times 10^{-6}\ T^2}$	$\boldsymbol{25 < T \leq 1170}$
$\boldsymbol{C_p = 650}$	$\boldsymbol{T > 1170}$
Thermal expansion 1/℃	
$\boldsymbol{\alpha = -9 \times 10^{-13}\ T^2 - 7.7 \times 10^{-9} T + 1.1 \times 10^{-5}}$	$\boldsymbol{25 < T \leq 1100}$
$\boldsymbol{\alpha = 1.8 \times 10^{-5}}$	T>1100
Elastic modulus GPa	
$\boldsymbol{E = 5.2 \times 10^{-5}\ T^2 - 0.088T + 1.6 \times 10^2}$	$\boldsymbol{25 < T \leq 798}$
$\boldsymbol{E = 3.1 \times 10^{-5}\ T^2 - 0.23T + 2.9 \times 10^2}$	$\boldsymbol{798 < T < 2500}$
Yield strength MPa	
$\boldsymbol{\sigma_Y = -9 \times 10^{-10}\ T^4 - 1.2 \times 10^{-6}\ T^3 + 0.00026\ T^2 - 0.23T + 3.2 \times 10^2}$	25<T<2500
Poisson's ratio	
$\boldsymbol{\nu = -4.8 \times 10^{-10}\ T^3 - 8.8 \times 10^{-7}\ T^2 - 0.00031T + 0.31}$	25<T<2500

Figures 4(a) and 4(b) demonstrate the predicted temperature profile for the sample with no preheating (sample 1 in Table 2), and with a pre-heating temperature of 100℃ (sample 2 in Table 2), respectively. The comparison of these plots shows that the overall temperature is higher for sample 2 which is preheated to 100℃, however, the temperature gradient is lower due to the preheating's effect and the fact that this preheating temperature would result in a higher rate of heat transfer and dissipation of heat through the material. Thus, looking at these figures, the residual stress is expected to be lower when the substrate is preheated to some level.

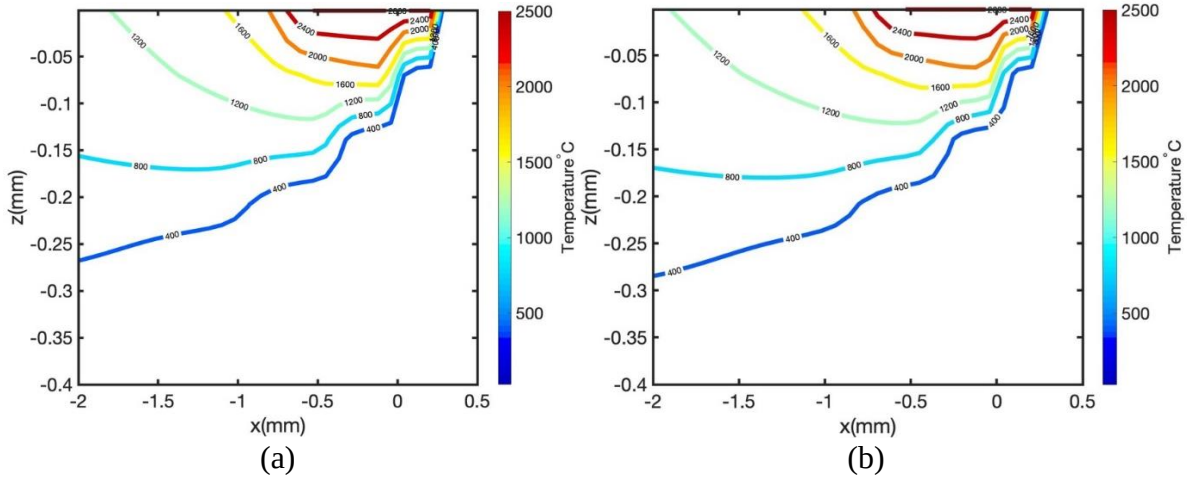

Figure 4. *Predicted Temperature profile for IN718 sample fabricated via L-PBF with (a) no pre-heating of the substrate (Sample 1 in Table 2) and (b) pre-heating of the substrate to 100℃ (Sample 2 in Table 2).*

Preprints (www.preprints.org) | NOT PEER-REVIEWED | Posted: 15 March 2021 doi:10.20944/preprints202103.0359.v1

Figure 5 and Figure 6 illustrate the predicted and measured residual stress along the scan direction (σ_x), and along the build direction (σ_z), respectively.

As shown in Figure 5, residual stresses at 5 different depths are calculated and compared to experimental measurements of residual stress for two cases where for one, the substrate is not preheated at all and, it is at ambient temperature, and for the other sample, the substrate is preheated to 100℃ . The black error bar shows the experimental residual stress measurements for no-pre-heating of the substrate, and the red one, shows the experimental measurements of residual stress for the case where the substrate is preheated to 100℃. The predicted residual stress shows that the tensile residual stress along the scan direction has dropped by half. Therefore, the preheating of the substrate has a substantial effect on residual stress build-up. The comparison of the predicted and measured residual stress for both samples are in good quantitative and qualitative agreements with the maximum error of 12%.

Figure 6 demonstrates the predicted and measured residual stress in the build direction. As shown in this figure, the residual stress in the build direction has reduced by around 14% when the substrate is preheated to 100℃.

The comparison of the results along the scan direction and build direction shows that the magnitude of residual stress along the build direction is higher than that along the scan direction. This observation is consistent with the experimental findings in and simulation results reported in [4].This is because the heat transfer is quite different in each direction due to the effect of heat loss. In addition, it is observed that pre-heating has more influence on residual stress along the scan direction compared to that along the build direction. This could be due to the fact that the microstructural evolution along the build direction and scan direction shows different behavior, thus affecting the material properties and residual stress formation.

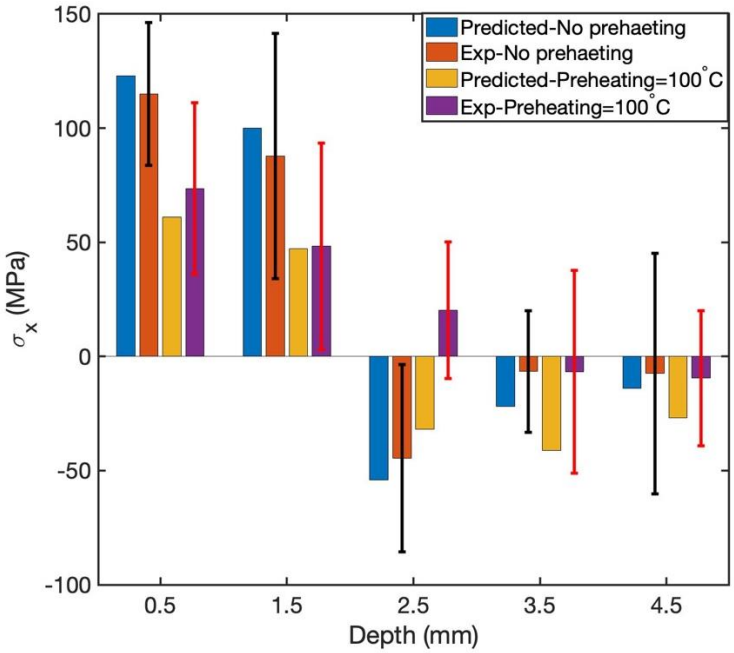

Figure 5.*Comparison of the predicted and measured residual stress along the scan direction.*

Preprints (www.preprints.org) | NOT PEER-REVIEWED | Posted: 15 March 2021 doi:10.20944/preprints202103.0359.v1

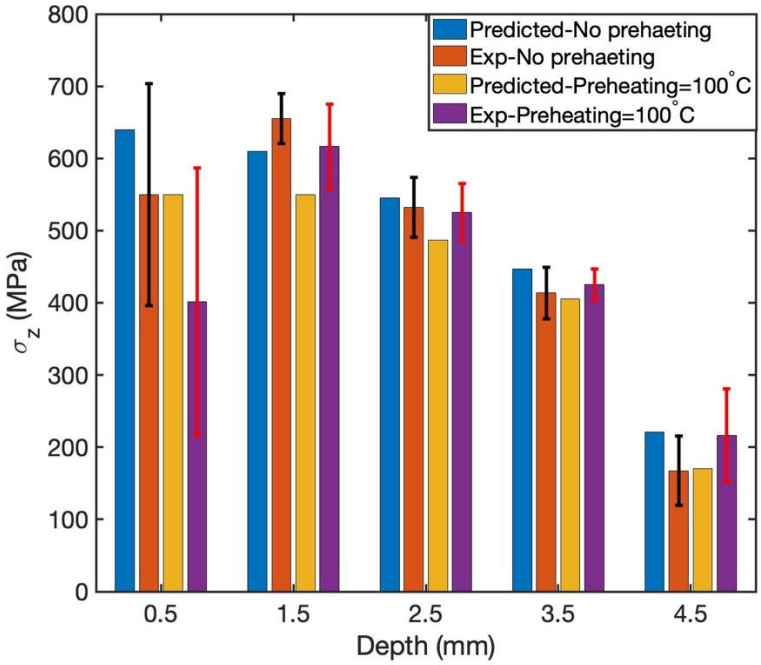

***Figure 6**. Comparison of the predicted and measured residual stress along the build direction.*

5. Sensitivity Analysis

Since the proposed model is validated, a sensitivity analysis is performed to investigate the effect of preheating in a broader range. In this sensitivity analysis the laser power is 150 W, the scan speed is 600 mm/s, the layer thickness is 30 μm, the hatching space is 100 μm, the number of scans is 50, and the preheating temperature ranges from 50℃ to 500℃. As it can be seen in Figures 7 and 8, the results show two different stages. One from 50℃ *to* 200℃ in which a rapid drop in residual stress is observed, and the second stage from 200℃ to 500℃ the residual stress has increased. This is due to the fact that at higher temperatures the melt pool and heat affected zone are large enough that build up high amount of shrinkage stress upon cooling. Moreover, the yield strength drops rapidly at higher temperatures and results in formation of larger residual stress. Therefore, the preheating has two impacts on residual stress; at lower preheating temperatures (in this case lower than 200℃), the preheating's effect on melt pool size is lower while decreasing the temperature gradient which would result in the decrease in residual stress; at higher preheating temperatures (in this case above 250℃), this high amount of preheating induces large enough melt pool zone that its impact on residual stress overweight its impact on the decrease in temperature gradient, thus would result in the increase in residual stress. It should be noted that the residual stress is highly tensile in the melt pool and heat affected zone as described previously in [5].
Thus, the results show the importance of the optimization of preheating temperature in achieving a desired residual stress and final performance of the manufactured part.

Preprints (www.preprints.org) | NOT PEER-REVIEWED | Posted: 15 March 2021 doi:10.20944/preprints202103.0359.v1

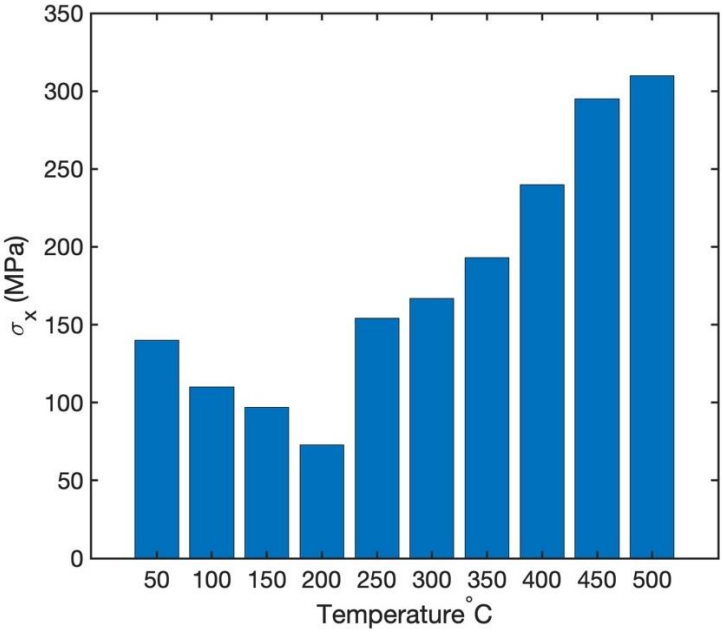

Figure 7. *Effect of pre-heating on residual stress build up in L-PBF of IN718 along the scan direction.*

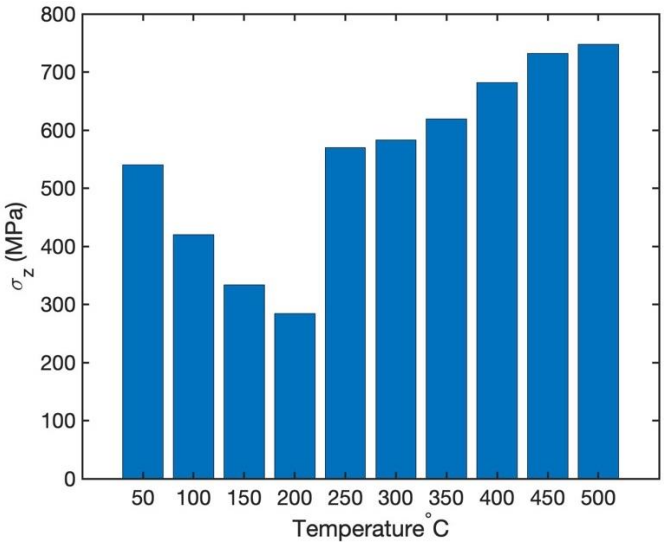

Figure 8. *Effect of pre-heating on residual stress build up in L-PBF of IN718 along the build direction.*

6. Conclusion

A physics-based analytical model is proposed to investigate the effect of preheating on residual stress build-up in L-PBF. The residual stress is predicted by calculating the temperature field using a moving point heat source approach by considering the effects of heat loss, temperature-dependent material properties, multi-layer and multi-scan aspects of the process, energy needed for solid-state phase change, and preheating temperature. The high-temperature gradient in this process induces high thermal stress which is calculated using Green's function of stresses due to the point body load. The thermal stress usually exceeds the yield strength of the material, thus a

consecutive model, known as the Johnson-Cook model is employed to capture the yield threshold. Then, as a result of cyclic rapid heating and cooling and the fact that the material is yielded and experiences the plasticity, the residual stress is calculated from incremental plasticity and kinematic hardening behavior of the metal.

The residual stresses are predicted for two cases where the substrate is at ambient temperature, and also for another case where the substrate is pre-heated. The results showed that residual stress decreased when the substrate is preheated. Moreover, the drop in residual stress along the scan direction was higher than that along the build direction. This is due to the fact that the heat transfer mechanisms and the subsequent microstructural evolution are quite different in these two directions resulting in variation of behaviors. The results are validated by fabricating samples under different preheating conditions using an L-PBF machine. X-ray diffraction was then used to measure the residual stress of the samples and then compared to predictions. Good quantitative and qualitative agreement is observed between predicted and measured residual stress.

In addition, a sensitivity analysis is performed to investigate the effect of preheating in a broader range. The results showed that the preheating temperature could reduce the residual stress, however, an excessive amount of preheating has an opposite impact on residual stress formation since this could result in reduction of yield strength due to the grain coarsening of the melt zone and heat-affected zone, thus increasing the residual stress build-up.

Acknowledgments: The experimental data were financially supported by the "Intelligent Manufacturing Research Center" (iMRC) from The Featured Areas Research Center Program within the framework of the Higher Education Sprout Project by the Ministry of Education (MOE) in Taiwan.

REFERENCES

1. Bartlett, J.L. and X. Li, *An overview of residual stresses in metal powder bed fusion.* Additive Manufacturing, 2019.
2. Bagg, S.D., L.M. Sochalski-Kolbus, and J.R. Bunn, *The effect of laser scan strategy on distortion and residual stresses of arches made with selective laser melting.* 2016.
3. Gu, D., *Laser additive manufacturing of high-performance materials*. 2015: Springer.
4. Ganeriwala, R., et al., *Evaluation of a thermomechanical model for prediction of residual stress during laser powder bed fusion of Ti-6Al-4V.* Additive Manufacturing, 2019. **27**: p. 489-502.
5. Mirkoohi, E., J.R. Dobbs, and S.Y. Liang, *Analytical modeling of residual stress in direct metal deposition considering scan strategy.* The International Journal of Advanced Manufacturing Technology, 2020. **106**(9-10): p. 4105-4121.
6. Sharma, R. and A. Kumar, *Track-Scale Simulations of Selective Laser Melting to Investigate Development and Mitigation of Thermal Stresses.* Lasers in Manufacturing and Materials Processing, 2019. **6**(4): p. 464-492.
7. Cao, J., M.A. Gharghouri, and P. Nash, *Finite-element analysis and experimental validation of thermal residual stress and distortion in electron beam additive manufactured Ti-6Al-4V build plates.* Journal of Materials Processing Technology, 2016. **237**: p. 409-419.

8. Lin, Y.-C. and K. Lee, *Effect of preheating on the residual stress in type 304 stainless steel weldment.* Journal of materials processing technology, 1997. **63**(1-3): p. 797-801.
9. Mirkoohi, E., et al., *Three-dimensional semi-elliptical modeling of melt pool geometry considering hatch spacing and time spacing in metal additive manufacturing.* Journal of Manufacturing Processes, 2019. **45**: p. 532-543.
10. Tabei, A., et al., *Modeling of texture development in additive manufacturing of Ni-based superalloys.* The International Journal of Advanced Manufacturing Technology, 2019: p. 1-10.
11. Ji, X., et al., *Analytical modeling of post-printing grain size in metal additive manufacturing.* Optics and Lasers in Engineering, 2020. **124**: p. 105805.
12. Nickel, A., D. Barnett, and F. Prinz, *Thermal stresses and deposition patterns in layered manufacturing.* Materials Science and Engineering: A, 2001. **317**(1-2): p. 59-64.
13. Alimardani, M., E. Toyserkani, and J.P. Huissoon, *A 3D dynamic numerical approach for temperature and thermal stress distributions in multilayer laser solid freeform fabrication process.* Optics and Lasers in Engineering, 2007. **45**(12): p. 1115-1130.
14. Chew, Y., et al., *Thermo-mechanical model for simulating laser cladding induced residual stresses with single and multiple clad beads.* Journal of Materials Processing Technology, 2015. **224**: p. 89-101.
15. Ding, J., et al., *Thermo-mechanical analysis of Wire and Arc Additive Layer Manufacturing process on large multi-layer parts.* Computational Materials Science, 2011. **50**(12): p. 3315-3322.
16. Ali, H., et al., *In-situ residual stress reduction, martensitic decomposition and mechanical properties enhancement through high temperature powder bed pre-heating of Selective Laser Melted Ti6Al4V.* Materials Science and Engineering: A, 2017. **695**: p. 211-220.
17. Buchbinder, D., et al., *Investigation on reducing distortion by preheating during manufacture of aluminum components using selective laser melting.* Journal of laser applications, 2014. **26**(1): p. 012004.
18. Sames, W.J., et al., *The metallurgy and processing science of metal additive manufacturing.* International Materials Reviews, 2016. **61**(5): p. 315-360.
19. Carslaw, H.S. and J.C. Jaeger, *Conduction of heat in solids.* Oxford: Clarendon Press, 1959, 2nd ed., 1959.
20. Ning, J., et al., *Analytical modeling of 3D temperature distribution in selective laser melting of Ti-6Al-4V considering part boundary conditions.* Journal of Manufacturing Processes, 2019. **44**: p. 319-326.
21. Mirkoohi, E., et al., *Thermo-mechanical modeling of thermal stress in metal additive manufacturing considering elastoplastic hardening.* CIRP Journal of Manufacturing Science and Technology, 2020. **28**: p. 52-67.
22. Kobayashi, T., et al., *Plastic flow behavior of Inconel 718 under dynamic shear loads.* International Journal of Impact Engineering, 2008. **35**(5): p. 389-396.
23. McDowell, D., *An approximate algorithm for elastic-plastic two-dimensional rolling/sliding contact.* Wear, 1997. **211**(2): p. 237-246.
24. Nadammal, N., et al., *Influence of support configurations on the characteristics of selective laser-melted inconel 718.* JOM, 2018. **70**(3): p. 343-348.
25. Prevey, P.S., *X-ray diffraction residual stress techniques.* ASM International, ASM Handbook., 1986. **10**: p. 380-392.

 doi:10.20944/preprints202103.0359.v1

26. Yang, Y., et al., *Prediction of microstructure, residual stress, and deformation in laser powder bed fusion process.* Computational Mechanics, 2018: p. 1-17.